Please cite this article in press as: Miallau et al., Comparative Proteomics Identifies the Cell-Associated Lethality of *M. tuberculosis* RelBE-like Toxin-Antitoxin Complexes, Structure (2013), http://dx.doi.org/10.1016/j.str.2013.02.008

Structure
Article

# Comparative Proteomics Identifies the Cell-Associated Lethality of *M. tuberculosis* RelBE-like Toxin-Antitoxin Complexes

Linda Miallau,[1,3,4] Paras Jain,[2,3] Mark A. Arbing,[1] Duilio Cascio,[1] Tung Phan,[1] Christine J. Ahn,[1] Sum Chan,[1] Irina Chernishof,[1] Michelle Maxson,[2] Janet Chiang,[1] William R. Jacobs, Jr.,[2] and David S. Eisenberg[1,*]
[1]Howard Hughes Medical Institute and UCLA-DOE Institute for Genomics and Proteomics and Department of Biological Chemistry, University of California, Los Angeles, Los Angeles, CA 90095-1570, USA
[2]Howard Hughes Medical Institute, Department of Microbiology and Immunology, Albert Einstein College of Medicine, Bronx, NY 10461, USA
[3]These authors contributed equally to this work
[4]Present address: Biochemistry Department, Uniformed Services University of the Health Sciences, Bethesda, MD 20814, USA
*Correspondence: david@mbi.ucla.edu
http://dx.doi.org/10.1016/j.str.2013.02.008

## SUMMARY

**The *Mycobacterium tuberculosis* (*Mtb*) genome encodes approximately 90 toxin-antitoxin protein complexes, including three RelBE family members, which are believed to play a major role in bacterial fitness and pathogenicity. We have determined the crystal structures of *Mtb* RelBE-2 and RelBE-3, and the structures reveal homologous heterotetramers. Our structures suggest RelE-2, and by extension the closely related RelE-1, use a different catalytic mechanism than RelE-3, because our analysis of the RelE-2 structure predicts additional amino acid residues that are likely to be functionally significant and are missing from analogous positions in the RelE-3 structure. Toxicity assays corroborate our structural findings; overexpression of RelE-3, whose active site is more similar to *Escherichia coli* YoeB, has limited consequences on bacterial growth, whereas RelE-1 and RelE-2 overexpression results in acute toxicity. Moreover, RelE-2 overexpression results in an elongated cell phenotype in *Mycobacterium smegmatis* and protects *M. tuberculosis* against antibiotics, suggesting a different functional role for RelE-2.**

## INTRODUCTION

Toxin-antitoxin (TA) systems were initially identified as important mediators of the stability of low-copy plasmids and of bacteriophage genomes in bacterial cells (Ogura and Hiraga, 1983; Gerdes et al., 1986). Similar systems have since been identified on the chromosomes of many archaea and bacteria, where they are believed to mediate an organism's response to physiological stresses (Pandey and Gerdes, 2005; Makarova et al., 2009). Typically, TA genes are organized as operons in which the first open reading frame (ORF) usually encodes an antitoxin and the second ORF encodes its cognate toxin (Van Melderen et al., 1994). Under optimal physiological conditions, the toxin and antitoxin form a stable complex that has no deleterious effects on the bacterial cell. Environmental stress, such as starvation, elevated temperature, or antibiotic exposure, can result in the proteolytic degradation of the labile antitoxin, allowing the stable toxin to exert a bacteriostatic or bacteriocidal effect on the bacterium (Pandey and Gerdes, 2005). Many families of toxins have been identified and each family appears to have a distinct mechanism by which it affects cellular growth, although there is considerable overlap in the cellular processes that are targeted for disruption. For instance, both the RelBE and MazEF systems target protein synthesis but use distinct mechanisms; RelE toxins inhibit translation in a ribosome-dependent manner by cleaving messenger RNAs (mRNAs) positioned at the ribosomal A-site (Pedersen et al., 2003; Christensen-Dalsgaard and Gerdes, 2008), whereas MazF degrades free mRNA (Zhang et al., 2003). Whereas toxins have a sole function (i.e., to mediate toxicity), antitoxins have the dual function of neutralizing the toxin through a C-terminal protein-protein interaction domain and acting as regulatory systems of their own TA operon through their N-terminal DNA-binding domain (Li et al., 2008).

The regulation of microbial physiology by TA systems has been widely discussed and many possible functions for TA systems have been proposed. However, the hypothesis that TA systems invoke a reversible bacteriostatic state in response to adverse environmental conditions has become more prevalent. The complete range of environmental stresses that activate TA systems is unknown, but the most biomedically significant may be bacterial persistence upon antibiotic exposure (Vázquez-Laslop et al., 2006; Maisonneuve et al., 2011).

The *Mycobacterium tuberculosis* (*Mtb*) genome contains about 90 TA systems, which may correlate with its propensity for persistence, a well-known phenomenon in human tuberculosis infections (Pandey and Gerdes, 2005; Ramage et al., 2009). The distribution of TA systems within the *Mtb* genome is markedly biased toward one particular TA system superfamily, the VapBC family, with over 45 of these systems present for which a growing number of structures are available (Miallau et al., 2009; Min et al., 2012). The remaining systems include members of the MazEF, HigBA, ParDE, and RelBE families. There are three representatives of the RelBE family encoded in

Please cite this article in press as: Miallau et al., Comparative Proteomics Identifies the Cell-Associated Lethality of *M. tuberculosis* RelBE-like Toxin-Antitoxin Complexes, Structure (2013), http://dx.doi.org/10.1016/j.str.2013.02.008



**Table 1. Data Collection Statistics for *Mtb* RelBE-2 and RelBE-3 TA Complexes**

| Data Collection | RelBE-2 (SeMet Labeled) | RelBE-3 (SeMet Labeled) | RelBE-3 (Native) |
|---|---|---|---|
| Wavelength (Å) | 0.9793 | 0.9717 | 0.9717 |
| Resolution (Å) | 2.0 | 2.5 | 2.15 |
| Space group | $P2_12_12_1$ | C2 | $P2_1$ |
| Unit cell | a = 75.5 Å, b = 79.5 Å | a = 135.9 Å, b = 41.2 Å, c = 68.8 Å | a = 42.2 Å, b = 187.3 Å, c = 113.9 Å |
| | c = 86.3 Å | β = 95.5° | β = 94.4° |
| Completeness (%) | 95.9 (100) | 94.4 (93.9) | 89.8 (90.4) |
| Multiplicity | 12.6 (13.0) | 1.8 (1.8) | 2.2 (2.1) |
| $\langle I \rangle / \langle \sigma(I) \rangle$ | 19.8 (4.6) | 13.9 (5.5) | 11.5 (1.9) |
| $R_{sym}$ (%) | 12.6 (54.3) | 3.3 (11.3) | 5.3 (40.2) |
| Number of selenium atoms per asymmetric unit | Two observed of eight expected | Three observed of ten expected | |

Numbers in parentheses refer to a high-resolution bin of approximate width 0.09 Å.

the *Mtb* genome (Rv1246c-Rv1247c, RelBE-1; Rv2865-Rv2866, RelBE-2; and Rv3357-Rv3358, RelBE-3) and expression of the toxins upon infection of human macrophages and inhibition of bacterial growth within the macrophage has been shown (Korch et al., 2009). Amino acid starvation results in proteolytic degradation of the RelB-like antitoxin by Lon protease and has two effects: first, degradation of RelB leads to activation of the transcription of the RelBE operon, and second, unsequestered RelE arrests cell growth through ribosome-dependent mRNA cleavage (Christensen and Gerdes, 2003; Korch et al., 2009). These toxins have also been linked to the development of *Escherichia coli* persisters resistant to a high dosage of antibiotics (Keren et al., 2004). Understanding the structure and function of the *Mtb* RelBE systems may reveal potential vulnerabilities of the *Mtb* cell and allow disruption of bacterial growth patterns, thus decreasing overall bacterial fitness.

Here, we present the crystal structures of the *Mtb* RelBE-2 and RelBE-3 complexes and a sequence comparison with RelBE-1. We show that all three toxins, RelE-1, RelE-2, and RelE-3, are functional and expressed during *Mtb* H37Rv infection of human macrophages. Our crystal structures reveal molecular details of TA interactions and show how the three RelBE TA systems differentially regulate *Mtb* growth and survival under various conditions. Our results highlight potential functional differences between toxins of the same superfamily and provide insight into the role of RelE toxins in promoting bacteriostasis, and hence survival, under adverse conditions.

## RESULTS

### Expression of Homologous *Mtb* RelE Toxins in *Mycobacterium smegmatis* Results in Differential Cell Growth Modulation

The electroporated *M. smegmatis* cells had two distinct cell growth characteristics (Figure S1 available online). Cells harboring the RelE-3-containing plasmid grew normally in the absence of the inducing agent and displayed a marked inhibition of growth in the presence of inducer characterized by the almost complete absence of colonies on the plates (Figure S1). In contrast, expression of the RelE-1 and RelE-2 toxins was highly toxic and no bacterial growth was observed on either the uninduced or induced plates, indicating that the leakiness of the promoter allowed a sufficient amount of toxin to be produced to inhibit cell growth (Figure S1). Control experiments in which the expression constructs were electroporated into the *M. smegmatis* $mc^2155$ strain, which lacks the T7 polymerase gene, displayed normal growth (data not shown), indicating that the growth phenotypes are toxin specific. Moreover, the observed toxin-mediated growth inhibition was alleviated by simultaneous expression of the antitoxins with their cognate toxins, indicating that growth inhibition is toxin specific and is not a nonspecific effect attributable to protein overexpression.

### Crystal Structures of the *Mtb* RelBE-2 and RelBE-3 Complexes

The *Mtb* RelE-like toxins are expected to have similar folds and characteristics based on a high percentage of sequence identity (RelE1-2 = 55%; RelE1-3 = 31%; RelE2-3 = 33%) (Figure S3). Because the cell-growth assays determined that RelE-1 and RelE-2 toxins are significantly more toxic than RelE-3 toxins, crystallographic studies were initiated to determine the structural basis of the differences in toxin toxicity. The structures of the RelBE-2 and RelBE-3 TA complexes were determined by selenomethionine (SeMet) single-wavelength anomalous diffraction (SAD) at a resolution of 2.0 and 2.5 Å, respectively (Supplemental Information). The RelBE-2 and RelBE-3 structures have excellent geometries. Data collection and refinement statistics are summarized in Tables 1 and 2.

The RelBE-2 and RelBE-3 TA complexes are tetrameric complexes of two toxins and two antitoxins. In each complex, one antitoxin binds a single toxin and the heterotetramer is formed almost exclusively by interactions between the antitoxins (Figure 1).

RelE-2 and RelE-3 toxins have a similar fold with a three-stranded β sheet surrounded by two α helices and a $3_{10}$ helix as the core structural element (Figure 2A). A structural comparison of the *Mtb* RelE-like toxins with proteins of known structure confirmed the prediction that the *Mtb* RelE-like toxins are members of the RelE/YoeB superfamily (see below for a detailed comparison).

The crystal structures of the RelB-2 and RelB-3 antitoxins reveal that these antitoxins have the same two-domain structure

**Table 2. Refinement Statistics for *Mtb* RelBE-2 and RelBE-3 TA Complexes**

| Refinement | RelBE-2 | RelBE-3 |
|---|---|---|
| Total number of molecules (toxin: antitoxin) per asymmetric unit | 4 (2:2) | 16 (8:8) |
| Protein residues | 352 out of 420 | 1,356 out of 1,400 + tags (168) |
| Solvent molecules | 173 | 439 |
| Heteroatoms | 40 | 0 |
| $R_{work}/R_{free}$ (%) | 20.3/24.6 | 21.5/26.1 |
| Rmsd bond lengths (Å)/bond angles (°) | 0.017/1.497 | 0.008/1.074 |
| Coordinate error based on R value (Å) | 0.163 | 0.3 |
| Ramachandran Analysis (%) | | |
| Favored regions | 94.4 | 96.9 |
| Additionally allowed regions | 4.9 | 3.1 |
| Generously allowed regions | 0.7 | 0.0 |
| Disallowed regions | 0.0 | 0.0 |

as members of the YefM antitoxin family (Kamada and Hanaoka, 2005; Kedzierska et al., 2007; Kumar et al., 2008). The N-terminal domain is a globular structure composed of a three-stranded β sheet surrounded by α helices α-1 and α-2 that extends into the C-terminal α-helical toxin-neutralization domain composed of α helices α-3, α-4, and α-5 (Figures 1A, 1F, and 2B).

Interactions between toxins and antitoxins in both the RelBE-2 and RelBE-3 complexes are mediated by antitoxin helices α-3, α-4, and α-5 with their respective toxins. The helices form an arm that surrounds the toxins and buries ~30% of the toxin's total surface area. These interactions are primarily electrostatic and involve numerous arginine residues from the toxins interacting with acidic antitoxin residues (Figures 1A, 1D, 1F, and 1I).

The two RelBE-2 and RelBE-3 heterodimers assemble with *C2* symmetry to form the heterotetrameric 2:2 antitoxin:toxin complexes (Figures 1A and 1F). The heterotetramers are exclusively formed through interactions of the antitoxins plus one additional hydrogen bond between the toxin and the opposing antitoxin in the RelBE-2 structure (Arg-62 NH2 and Gln-56 OE1, respectively) (Figures 1A and 1F). The N-terminal globular domains of the antitoxins interact nonspecifically to form an extended six-stranded β sheet that is highly hydrophobic (Figures 1B and 1G). Helices α-3 and α-3′ also contribute to the antitoxin dimer interface by interacting through hydrophobic residues. These helices cross at an angle of ~35° to form a funnel that accommodates large hydrophobic residues at the top of the funnel and smaller side chains at the bottom of the funnel (Figures 1A and 1F).

## Phylogenetic Clustering

RelE toxins belong to a diverse toxin superfamily that includes the RelE and YoeB toxins and has representatives in both the archaea and bacteria. Because the overall fold of RelE/YoeB toxins is conserved but protein function has significantly diverged (Arbing et al., 2010), we constructed a phylogenetic tree using sequences from those RelE-like proteins for which structures have been determined. The goal is to identify amino acid residues that may be important for toxin activity (Figures 3A and 3B). The toxins assemble in two main clusters: the first one contains the three *Mtb* RelE-like proteins and *E. coli* YoeB (*Ec*YoeB) while the second comprises the archaeal RelE toxins and *E. coli* RelE (*Ec*RelE). Within the first cluster, *Mtb* RelE-1 and RelE-2 toxins form a distinct subcluster while *Mtb* RelE-3 is located in a second subcluster with the extensively characterized *Ec*YoeB, whose catalytic strategy has been elucidated (Christensen et al., 2001; Christensen and Gerdes, 2003). The relative distance among all three *Mtb* RelE-like proteins within the primary cluster indicates a possible divergence in catalytic mechanisms and target of action.

## Structural Homolog Comparison of RelBE-3

Superposition of the structures of *Mtb* RelE-3 with *Ec*YoeB (Protein Data Bank [PDB] code 2A6Q) shows a root-mean-square deviation (rmsd) of 2.4 Å for 78 α-carbon pairs with 26% sequence identity (Figure S2). The phylogenetic analysis suggests that RelE-3 is more similar to YoeB than to the other toxins of the RelE/YoeB superfamily. Consistent with this prediction is the conservation of the YoeB residues implicated in its catalytic mechanism (Zhang et al., 2003; Kamada and Hanaoka, 2005) in analogous positions in the RelE-3 toxin structure, which suggests that RelE-3 cleaves RNA in a similar manner as *Ec*YoeB. The catalytic mechanism of RelE-3 would involve Glu-47 acting as a general base and His-84 serving as the general acid. A large rearrangement of the C-terminal domain of RelE-3 upon antitoxin release would be required to bring Glu-47 and His-84 into favorable conformations for catalysis. Analogous to YoeB, the *Mtb* RelE-3 Arg-60 and/or Arg-65 residues would be involved in binding the RNA reactive phosphate group (Zhang and Inouye, 2009). RelE-3 may thus be an incomplete endoribonuclease that binds to the A-site of the 70S ribosome to cleave mRNA using a mechanism analogous to that of *Ec*YoeB.

The structural homology between the toxins of the RelBE-3 complex and the YefM-YoeB complex extends to the antitoxin structures as well (rmsd of 1.9 Å for the superposition of 74 Cα with a sequence identity of 24%). The RelBE-3 interactions are similar to those seen in the YefM-YoeB structure and thus RelB-3 inhibits RelE-3 in the same manner as YefM-YoeB.

## Structural Homolog Comparison of RelE-2

The phylogenetic tree (Figure 4A) based on sequence alignments (Figure 4B) suggests that RelE-1 and RelE-2 form a separate subcluster within their branch of the tree and thus may have diverged from the other toxins in the cluster in terms of a catalytic mechanism. A DALI search (Holm and Sander, 1995) using the coordinates for RelE-2 identified close structural relationships with *Ec*YoeB and *Ec*RelE toxins (Figures 4A and 4B) (Kamada and Hanaoka, 2005; Zhang and Inouye, 2009).

Structural comparisons reveal a lack of conservation of functionally important YoeB residues (Kamada and Hanaoka, 2005) in equivalent positions in RelE-2. However, the YoeB Arg-65 believed to bind the RNA reactive phosphate group is conserved in equivalent positions in *Mtb* RelE-1 and RelE-2 (Figure 4D; RelE-1 Arg-62 and RelE-2 Arg-61) and thus could also play this role in RelE-1 and RelE-2 (Figure S3). The nonconservation of the residues that act as the YoeB general acid and base in *Mtb*

Please cite this article in press as: Miallau et al., Comparative Proteomics Identifies the Cell-Associated Lethality of *M. tuberculosis* RelBE-like Toxin-Antitoxin Complexes, Structure (2013), http://dx.doi.org/10.1016/j.str.2013.02.008



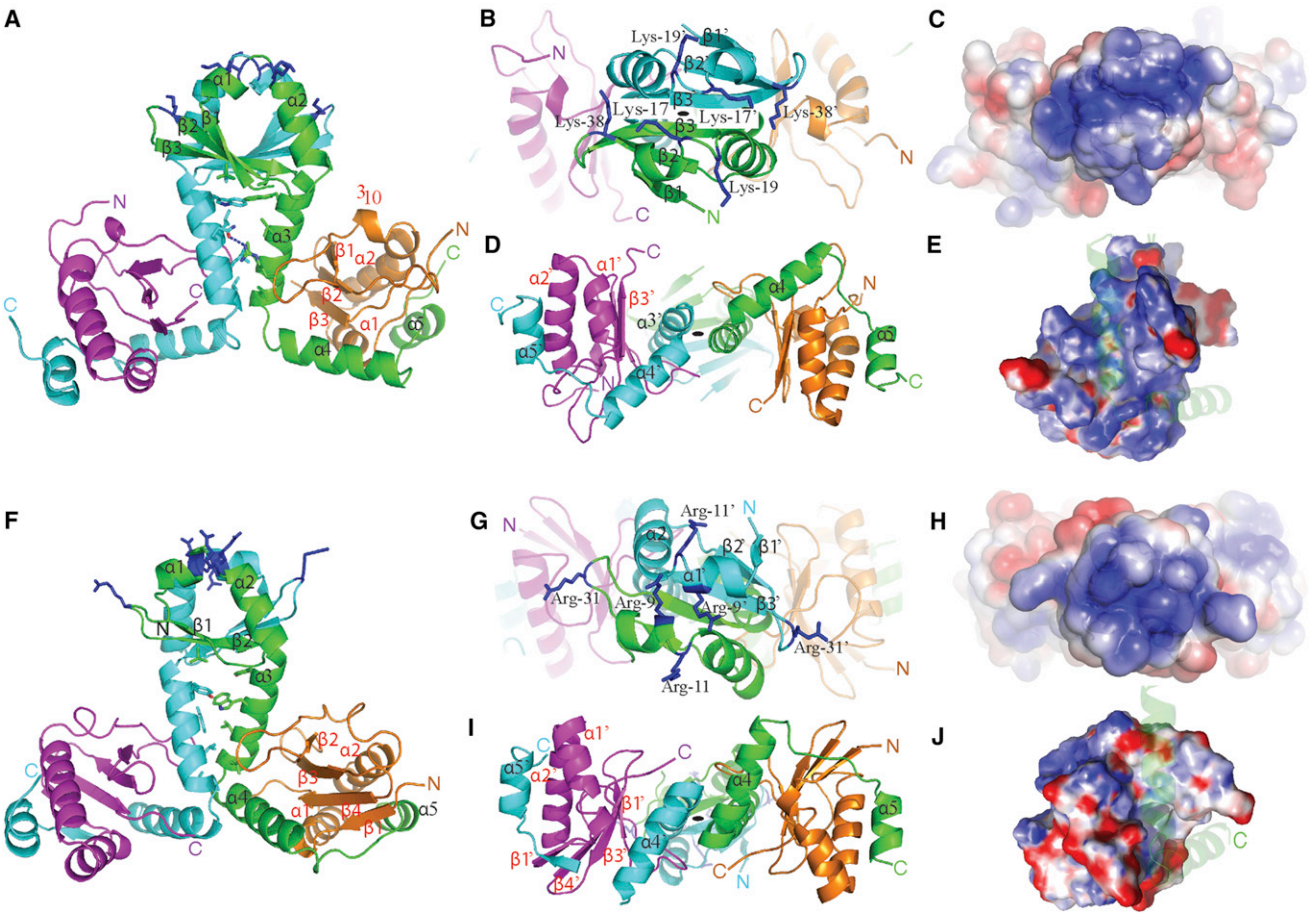


**Figure 1. The Structures of *Mtb* RelBE-2 and *Mtb* RelBE-3**

N and C termini are indicated by N or C, respectively. Antitoxins are shown in green and cyan and toxins are shown in magenta and orange. Secondary structure elements are marked with an apostrophe.

(A and F) Ribbon diagrams of the RelBE-2 and RelBE-3 heterotetramers, respectively. The single hydrogen bond formed between RelB-2 of one heterodimer and RelE-2 of the symmetry-related molecule is represented as a blue dotted line. Secondary structure annotations are shown in black for antitoxins and in red for toxins.

(B and G) Top view of the ribbon diagram of the heterotetramers. Conserved basic residues are likely to be involved in DNA binding are shown as blue sticks.

(C and H) Surface potential representation of the RelBE-2 and RelBE-3 heterotetramers showing the antitoxin DNA-binding domain.

(D and I) Bottom view of the ribbon diagrams showing antitoxin helices α-4 and α-5 that envelop the toxins.

(E and J) Ribbon diagram of RelE-2 and RelE-3 and stick representation of putative substrate binding and catalytic residues.

RelE-1 and RelE-2 suggests that these toxins use an alternative RNA cleavage mechanism consistent with the differences in toxin-mediated cell growth arrest seen in this study and that of Korch et al. (2009).

Our search for RelE-2 structural homologs also identified two archaeal RelE toxins, *Pyrococcus horikoshii* aRelE (PDB code 1WMI) and *Methanococcus jannaschii Mj*RelE (PDB code 3BPQ), whose structures were determined in complex with their cognate antitoxins aRelB and *Mj*RelB, respectively (Takagi et al., 2005; Francuski and Saenger, 2009).While the toxins share an equivalent core structure ($rmsd_{aRelE\text{-}RelE\text{-}2}$ = 1.8 Å, 75 Cα pairs, 27% sequence identity, Z score = 10.9; $rmsd_{MjRelE\text{-}RelE\text{-}2}$ = 2.2 Å, 72 Cα pairs, 22% sequence identity, Z score = 9.3), the antitoxins have a completely unrelated fold and therefore bind their cognate toxin partners in a different manner (Figure 4A). Strikingly, despite the differences in the fold and sequences of the Mtb and archaeal antitoxins, there is strong conservation of three of the five functionally important aRelE residues in analogous positions in all four toxins (Figures 4 and 5). These residues (RelE-1: Leu-49, Ser-58, and Arg-62; RelE-2: Leu-45, Ser-54, and Arg-61; aRelE: Leu-48, Arg-58, and Arg-65; *Mj*RelE: Ile-47, Arg-55, and Ser-62) mediate TA interactions and play key roles in the TA interface. The other two aRelE residues (Arg-40 and Arg-85) implicated as crucial for aRelE function are conserved in structurally analogous positions in RelE-1 (Arg-44 and Arg-85) and RelE-2 (Arg-40 and Arg-81). However, the side chains of these arginine residues do not strictly superimpose in the RelE-2 and aRelE structures, most likely because these are solvent exposed, disordered, and lacking observed density for the side-chain atoms (Figure 4A). An equivalent residue to aRelE Arg-40 is missing in *Mj*RelE but aRelE residue Arg-85 is conserved as Arg-80 in *Mj*RelE. It is noteworthy that

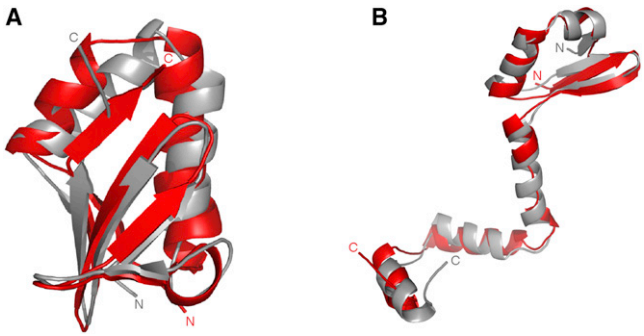


**Figure 2. Superposition of the Structures of *Mtb* RelE-like Toxins and *Mtb* YefM-like Antitoxins**

RelBE-2 is shown in red and RelBE-3 in gray.

(A) Ribbon diagram of the crystal structures of RelE-2 and RelE-3.

(B) Ribbon diagram of the crystal structures of RelB-2 and RelB-3.

in the structure of *Mj*RelE Arg-62, which is conserved in analogous positions in aRelE, *Mtb* RelE-1, and RelE-2 and proposed to mediate RNA cleavage, was spontaneously mutated to a serine. In the structure, *Mj*RelE Ser-62 does not directly interact with *Mj*RelB but an arginine side chain at this position would make a direct interaction with the antitoxin as observed in the aRelBE and *Mtb* RelBE-2 structures.

Further structural comparison of the structures of aRelE, *Mj*RelE, and *Mtb* RelE-2 in complex with their respective partners identifies two additional arginine residues that are conserved in all three structures (RelE-2: Arg-56 and Arg-77; RelE-1: Arg-57 and Arg-76; aRelE: Arg-60 and Arg-81; and *Mj*RelE: Arg-57 and Arg-76). aRelE Lys-47, *Mj*RelE Lys-45, and *Mtb* RelE-2 Lys-43 also interact with their cognate antitoxins and thus may play a role in mediating TA interactions (Figures 4A and 4B).

The structure of *Ec*RelE solved in complex with the *Thermus thermophilus* 70S ribosome (PDB code 3KIS) sheds light on the RelE-induced RNA cleavage mechanism (Neubauer et al., 2009). The overall structures of *Ec*RelE and the two *Mtb* RelE toxins are conserved ($rmsd_{EcRelE\text{-}MtbRelE\text{-}2}$ = 1.9 Å on 75 C$\alpha$, 20% sequence identity, *Z* score = 10.1; $rmsd_{EcRelE\text{-}MtbRelE\text{-}3}$ = 2.0 Å on 75 C$\alpha$, 16% sequence identity, *Z* score = 9.3) but only *Ec*RelE arginine residues Arg-61, which stabilizes the intermediate, and Arg-81, which acts as a general acid, are strictly conserved in *Mtb* RelE-1 and RelE-2 (corresponding residues: RelE-1, Arg-62 and Arg-80; RelE-2, Arg-61 and Arg-81) (Figure 4; Figure S3).

## RelE-2 Expression Results in Altered Mycobacterial Cell Morphology

Expression of *Mtb* RelE-1 and RelE-2 toxins have similar effects on cell viability (Figure S1) and sequence alignments suggest that these toxins share a common catalytic mechanism and are likely to be functionally redundant. To further explore the effects of this subclass of RelE toxins on mycobacterial physiology, we examined the effects of RelE-2 expression. The RelE-2 toxin was successfully expressed in *M. smegmatis*, a tractable mycobacterial model system. The control strain grew normally and the cell morphology was consistent with typical *M. smegmatis* cell morphology (Figure 5A). RelE-2 expression was found to result in abnormal cell growth characterized by the presence of elongated filamentous cells about 2.5 times the length of normal *M. smegmatis* cells (Figure 5B; Movie S1). Coexpression of the RelB-2 antitoxin resulted in normal cell morphology, indicating the effect is toxin mediated (Figure 5C).

## RelE-2 Expression Enhances Mycobacterial Survival upon Antibiotic Exposure

The influence of RelE-2 expression on *M. smegmatis* drug tolerance was evaluated by exposing the cells to lethal doses of the antituberculous antibiotics ofloxacin (OFX), rifampicin (Rif), or isoniazid (INH). Strikingly, expression of RelE-2 in cells exposed to a lethal dose of OFX (ten times the minimum inhibitory concentration) resulted in a 100-fold increase in the number of viable cells at 30 hr after antibiotic exposure (Figure 6A). RelE-2 expression had only a modest effect on cell survival at the 30 hr time point for cells exposed to the antibiotics Rif and INH. However, there was a significant effect on the killing kinetics compared to the cells harboring the empty expression vector (Figures 6B and 6C). A 10-fold increase in survival was observed for the RelE-2-expressing cells exposed to both Rif and INH during the first 20 hr of the respective treatments, but at the end of the 30 hr time course a similar decrease in the colony-forming unit of the cells was observed for both drugs. To verify that the increased survival rate was RelE-2 dependent, a *Mtb* H37Rv *RelE-2* deletion mutant was constructed by specialized transduction (Bardarov et al., 2002) and the effect of the *RelE-2* deletion on cell survival upon antibiotic exposure was determined (Figures 6D–6F). OFX or a combination treatment of INH and Rif resulted in a log-lower survival at the end of 4 days for Δ*RelE-2* in comparison to H37Rv (Figures 6E and 6F). However, no difference in the killing kinetics of Δ*RelE-2* in comparison to H37Rv was observed after INH or Rif treatment. Because it has been documented that *rel* homologs are expressed after infection of *Mtb* in macrophages (Korch et al., 2009), $mc^2$3403 (expresses an empty vector), $mc^2$3404 (expresses RelE-2), and $mc^2$3405 (expresses RelBE-2) strains were used to infect a human acute monocytic leukemia THP.1 cell line (Figure 7). In the uninduced condition, all three strains resulted in a similar macrophage death as determined by subG1 analysis. A short induction of either RelE-2 or RelBE-2 decreased the macrophage cell death from 72.2% ($mc^2$3403) to 33% ($mc^2$3404) and 25.9% ($mc^2$3405), respectively. A longer induction of RelE-2 or RelBE-2 did not significantly alter the result compared to the short induction and cell death of 79.3%, 40.1%, and 37.8% was observed in cells infected with $mc^2$3403, $mc^2$3404, and $mc^2$3405, respectively.

## DISCUSSION

Our structures of the *Mtb* RelBE family of complexes reveal that the overall folds of the individual toxins and antitoxins are well conserved with the superfamilies RelE/YoeB and YefM, respectively, to which these proteins belong (Francuski and Saenger, 2009). The overall architecture of the *Mtb* complexes is also conserved as revealed by the heterotetrameric crystal structures of RelBE-2 and RelBE-3. However, significant differences in putative catalytic residues of the toxins, identified by structural

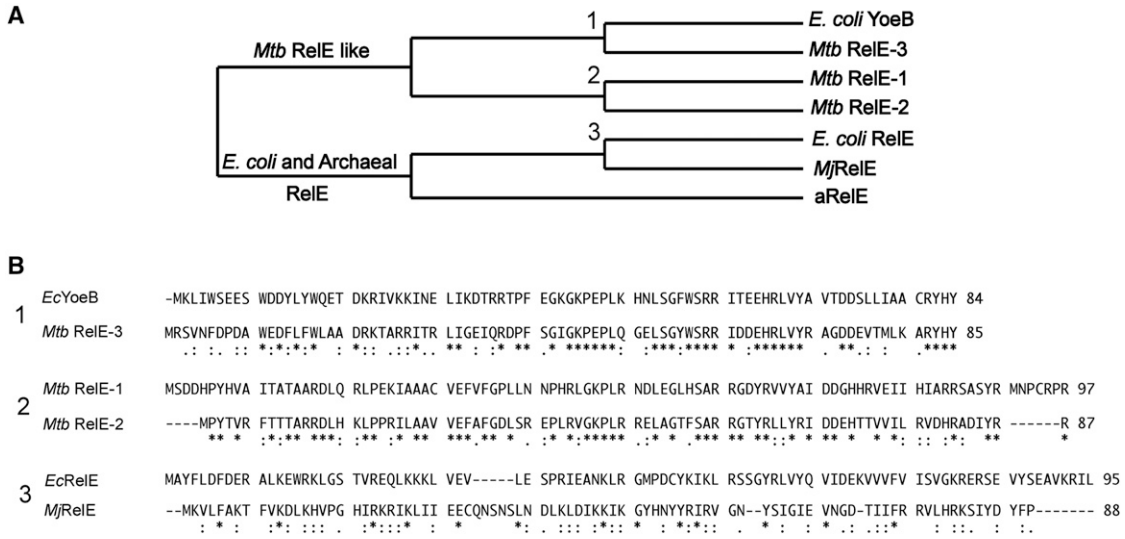


**Figure 3. Phylogenetic Tree of RelE-like Protein Homologs based on Protein Sequence Multialignment**

(A) A phylogenetic tree was generated from a multiple sequence alignment prepared with CLUSTALW (Thompson et al., 1994) using the Phylogeny.fr server (Dereeper et al., 2008).

(B) Sequence alignment corresponding to the three main clusters of the phylogenetic tree.

and sequence comparisons, suggest that RelE-1 and RelE-2 employ a distinct catalytic mechanism from their closely related counterpart RelE-3 to exert toxicity.

The dimeric N-terminal domains of the RelB-2 and RelB-3 antitoxins, as in the structurally homologous YefM and Phd antitoxins, form a positively charged structure consistent with the reported DNA-binding activity of the antitoxins that is required for autoregulation of transcription of the TA operon (Kamada and Hanaoka, 2005; Garcia-Pino et al., 2010). Structural alignments of our RelB-2 and RelB-3 structures and the sequence comparison with *Mtb* RelB-1 show the conservation of arginine residues in RelB-3 and RelB-1 and lysine residues in RelB-2, at equivalent positions (Figures 1A, 1B, 1F, 1G, and 2B). The substitution of lysine residues, whose acetylation results in stronger DNA binding and more stringent control of operon expression (Bahassi et al., 2011), for arginine residues may be a biological adaptation used by *Mtb* to modulate activity of the numerous TA complexes encoded within its genome.

Despite dramatic differences in backbone fold and sequence of the antitoxins that neutralize RelE-like toxins in the complex structures of *Mtb* RelBE-2, *P. horikoshii* aRelBE and *M. jannaschii Mj*RelBE, the same conserved toxin residues are shielded in the interaction (Figures 4C and 4D). We can postulate that these residues are not only conserved because they mediate the protein-protein interactions governing TA complex formation but that they may also be involved in RNA substrate binding and/or in the catalytic activity of these RelE ribonucleases. Although RelE has been shown to require association with the ribosome for full activity, it is likely that crucial residues involved in the catalytic mechanism of RNA degradation may still need to be protected to prevent nonspecific RNA degradation (Christensen and Gerdes, 2003). We propose that *Mtb* RelE-2 Arg-56 and Arg-61, which are also conserved in *Mtb* RelE-1 as Arg-60 and Arg-65, are likely to be involved in stabilizing the negative charge of the RNA phosphate groups, as shown by a spontaneous mutation, that abolish the toxicity of *Mj*RelE. Additional residues, identified through structural comparisons, likely to be involved in RelE-like protein toxicity are RelE-2 Lys-43, Leu-45, Ser-54, and Arg-77. It is noteworthy that these residues are also conserved in *Mtb* RelE-1, but the lack of crystal structure for the *Mtb* RelBE-1 complex prevents us from describing the TA interactions in detail (Figure 4D).

The filamentation/elongation of *Mtb* was previously observed for cells growing in macrophages after infection (Chauhan et al., 2006) and correlates well with the expression profile of *rel* genes during intracellular growth (Korch et al., 2009). Inhibition of macrophage cell death after *Mtb* infection plays a central role in tuberculosis disease pathogenesis (Hinchey et al., 2007). Our observation that *M. smegmatis* expressing *Mtb* RelE-2 toxin suppresses macrophage-mediated bacterial cell death suggests that this TA system may represent another *Mtb* cell-death suppression mechanism. The observed phenotype suggests that RelE-2 may target RNAs encoding proteins involved in cell division, thus resulting in elongated cells (Figure 5B). However, further work is required to determine the role of RelE-2 in cell elongation, the prevention of macrophage cell death, and intracellular *Mtb* survival.

The large diversity in the families of TA complexes rises from partner switching allowed by the modularity in antitoxin structure. The folds of the *Mtb* RelE-like toxins are very similar to both archaeal and bacterial RelE-like toxins. However, the folds of the *Mtb* RelB-1, RelB-2, and RelB-3 antitoxins are completely unrelated to the RelB proteins of the archaeal and bacterial RelBE systems and are instead structurally similar to the YefM-like antitoxins. The RelBE-2 and RelBE-3 complexes are thus derived from mixing between major classes of the RelE superfamily of toxins and the PhD/YefM antitoxin superfamily (Anantharaman and Aravind, 2003).

Our toxicity data show that *Mtb* RelE-like proteins are not equally toxic and these differences can be attributed to the

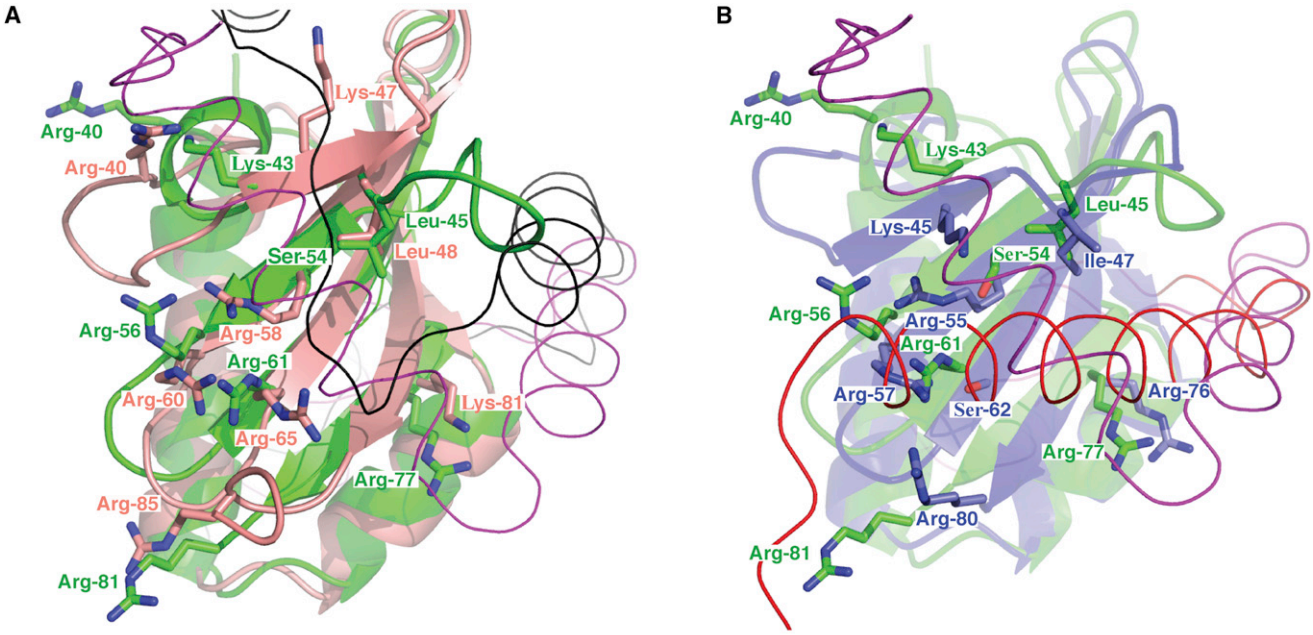


C

```
aRelE          1  MTYRVKIHKQ  VVKALQSLPK  AHYRRFLEFR  D-ILEYEPVP  REKFDVIR-L  EGTGDLDLYR  ARLGDYRVIY  SVNWKDKVIK  ILRLKPRGRA  YK          88
Mtb RelE-2     1  VPYTVRFTTT  ARRDLHKLPP  RILAAVVEFA  FGDL-----S  REPLRVGKPL  RREL-AGTFS  ARRGTYRLLY  RIDDEHTTVV  ILRVDHRADI  YRR         87
MjRelE         1  --MKVLFAKT  FVKDLKHVPG  HIRKRIKLII  EECQ-NSNSL  NDLKLDIKKI  KGY--HNYYR  IRVGNYSIGI  EVNGD--TII  FRRVLHRKSI  YDYFP       88
Mtb RelE-1     5  HPYHVAITAT  AARDLQRLPE  KIAAACVEFV  FGPLLN----  -NPHRLGKPL  RNDL-EGLHS  ARRGDYRVVY  AIDDGHHRVE  IIHIARRSAS  YRMNPCRPR   90
                     * :       ::*  :*          :              * :          :   * * **::          :   : ::  *
```

D

| aRelE | MjRelE | MtbRelE-2 | MtbRelE-1 | EcRelE | Putative Function |
|---|---|---|---|---|---|
| Arg-40 | NC | Arg-40 | Arg-44 | NC | crucial |
| Lys-47 | Lys-45 | Lys-43 | Lys-47 | NC | RNA binding |
| Leu-48 | Ile-47 | Leu-45 | Leu-49 | NC | crucial |
| Arg-58 | Arg-55 | Ser-54 | Ser-58 | NC | crucial |
| Arg-60 | Arg-57 | Arg-56 | Arg-57 | NC | RNA binding |
| Arg-65 | Ser-62(R62S) | Arg-61 | Arg-62 | Arg-61 | RNA cleavage |
| Lys-81 | Arg-76 | Arg-77 | Arg-76 | NC | RNA binding |
| Arg-85 | Arg-80 | Arg-81 | Arg-80 | Arg-81 | RNA cleavage |

**Figure 4. Superposition of the Structure of *Mtb* RelBE-2 with Its Structural Homologs**

In all figures, *Mtb* RelB-2 is shown in magenta, *Mtb* RelE-2 is in green, aRelE is in pink, aRelB is in black, *Mj*RelE is in blue, and *Mj*RelB is in red. Functionally important residues are shown as green (*Mtb* RelE-2), pink (aRelE), or blue sticks (*Mj*RelE).

(A) Superposition of *Mtb* RelBE-2 and aRelBE.

(B) Superposition of *Mtb* RelBE-2 and *Mj*RelBE.

(C) Structure-based sequence alignment of *Mtb* RelE-2 with aRelE, *Mj*RelE, and *Mtb* RelE-1. Side chains of the residues that interact with the antitoxins are shown in bold and colored according to the structure to which they belong. The red boxes highlight residues for which interactions with the antitoxins are conserved.

(D) Summary of the residues that are conserved in the structures of aRelE, *Mj*RelE, *Mtb* RelE-2, RelE-1, and *Ec*RelE. Shaded rows highlight residues that interact with residues of the antitoxins. Residues shown to be crucial for toxicity in other studies are indicated in the last column.

NC, not conserved. See also Figures S2 and S3.

variation in functionally important catalytic residues. RelE-3 is likely to use a similar mechanism as *Ec*YoeB, with RelE-3 residues Glu-47 and His-84 serving as the general acid and base and Arg-60 and/or Arg-65 binding the RNA reactive phosphate group (Kamada and Hanaoka, 2005; Figure 4D). In our *M. smegmatis* toxicity experiment, RelE-3 expression was shown to be mildly toxic, only slightly retarding cell growth, which correlates with the limited effect of YoeB expression on the colony-forming ability of wild-type *E. coli* (Christensen et al., 2004). *Mtb* RelE-1 and RelE-2 have catalytic residues conserved in analogous positions and are both extremely toxic, suggesting that they share a common mechanism. In vivo *Mtb* killing assays indicate that these toxins may be functionally redundant because no difference in the killing kinetics of the mutant compared to the wild-type was observed in the Δ*relE-2* strain to INH and Rif (Figures 6E and 6F). However, the presence of expressed RelE-2 is advantageous to *Mtb* because it protects the cells against the antibiotics Rif and INH for short periods of up to 20 hr (Figures 6B and 6C) and RelE-2-expressing *M. smegmatis* had higher short-term survival rates in macrophages (Figure 7). Considering the redundancy of toxin-encoding genes in the *Mtb* genome, it is not surprising that the suppression of one toxin gene has little effect. However, the short-term protection against antibiotics after RelE-2

Please cite this article in press as: Miallau et al., Comparative Proteomics Identifies the Cell-Associated Lethality of *M. tuberculosis* RelBE-like Toxin-Antitoxin Complexes, Structure (2013), http://dx.doi.org/10.1016/j.str.2013.02.008



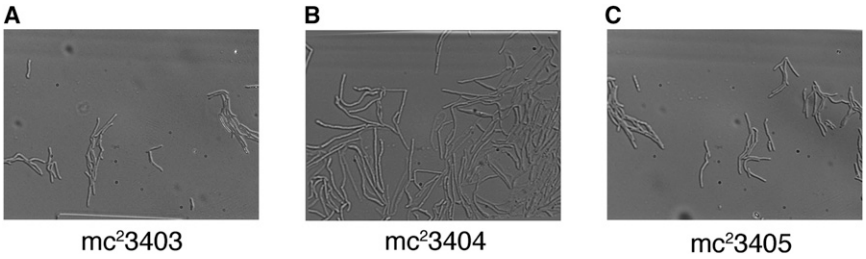


**Figure 5. Micrographs of *M. smegmatis* Cells**

(A) Control: *M. smegmatis* mc²3403 expressing the empty pYUB1485 vector.

(B) Expression of RelE-2 (mc²3404) results in cell elongation in *M. smegmatis*.

(C) The elongation phenotype upon RelE-2 expression is neutralized by RelB-2 coexpression (mc²3405).

See also Figure S1.

overexpression may not accurately reflect the in vivo effects of stress-induced toxin expression. It is likely that the survival capability of *Mtb* is linked to a network of mechanisms for which each individual toxin may make only a modest contribution.

Our studies have revealed the structural similarities of the *Mtb* RelE-like TA systems and have highlighted the specific structural features that are the basis for the differences in toxicity seen between RelE-3, which is only mildly toxic, and RelE-2 and RelE-1, which are acutely toxic. RelE-2 expression was found to have an effect on cell division, resulting in elongated cells, which is likely linked to the decreased antibiotic susceptibility of RelE-2-expressing cells. Similar to other TA complexes, the antitoxin molecules interact with their toxins so as to occlude the catalytic residues of the toxins and thus prevent accidental toxicity.

The variations in toxin-mediated toxicity between structurally related toxin family members may allow for fine-tuning of the bacterial response to different stresses and/or regulatory controls, thus resulting in toxin-dependent effects on microbial growth. If the functional diversity of the *Mtb* RelE-like toxin family is extended to the other TA systems encoded in the *Mtb* genome, then it would form an extremely complex stress-response network that is likely the key component of the ability of *Mtb* to respond and adapt to the transiently harsh environment in which it resides.

## EXPERIMENTAL PROCEDURES

### Construction of the RelBE-2 and RelBE-3 Coexpression Vectors

The individual genes encoding the RelBE-2 or RelBE-3 TA complexes were cloned into the pET46-Ek/LIC plasmid using the LIC minimal adaptor (both from Novagen, Gibbstown, NJ) such that toxin and antitoxin are coexpressed from the same vector with a cleavable affinity tag appended to the toxin. Additional description of cloning procedures is provided in Supplemental Information.

### Protein Expression and Purification

SeMet-labeled RelBE-2 complex was produced by following the protocol of Van Duyne et al. (1993). Complex expression in *E. coli* BL21(DE3) was induced by 1 mM IPTG for 5 hr at 37°C. The cell pellet was resuspended in buffer A (20 mM Tris [pH 8.0], 300 mM NaCl, 10 mM imidazole, 10% glycerol containing 1X Bugbuster [Novagen, Gibbstown, NJ]) and lysed using a French press. The complex was purified by Ni-NTA affinity chromatography and the pure SeMet-labeled RelBE-2 complex concentrated to 6 mg/ml for crystallization screening.

Native and SeMet-labeled RelBE-3 complexes were both produced in *E. coli* Rosetta (DE3). SeMet-labeled RelBE-3 was produced using the protocol of Van Duyne et al. (1993). Protein expression was induced by the addition of IPTG to 0.75 mM or 1 mM and cells grown for 5 hr at 37°C or overnight at 20°C for SeMet-labeled and native protein complexes, respectively.

Cell pellets for both native and SeMet-labeled RelBE-3 protein complexes were resuspended in buffer C (20 mM Tris [pH 8.0], 300 mM NaCl, 10 mM imidazole, and 10% glycerol) and lysed by French press. The complexes were purified by Ni-NTA affinity chromatography and then dialyzed against 20 mM HEPES (pH 8.0), 300 mM NaCl, and 10% glycerol. Reductive methylation of the native complex was then performed (Shaw et al., 2007). The complexes were further purified using a Superdex S-200 equilibrated in buffer E (buffer C without imidazole) and were concentrated to 20 mg/ml for crystallization screening. Additional details on protein expression and purification are described in Supplemental Information.

### Crystallization and Data Collection

Diffraction quality crystals of SeMet RelBE-2 were obtained in 25% PEG MME 2,000 and 0.15 M potassium thiocyanate. Strongly diffracting crystals of SeMet RelBE-3 were obtained using 0.1 M Tris (pH 8.9), 0.1 M NaCl, 24% PEG 10,000, and 20% glycerol at a protein concentration of 7 mg/ml. Diffraction quality crystals of the methylated native RelBE-3 complex were obtained in 0.1 M sodium citrate tribasic dehydrate (pH 5.6), 20% 2-propanol, and 20% w/v PEG 4,000. All crystals were flash frozen in liquid nitrogen and data were collected at beamline 24-ID-C of the Advanced Photon Source (Table 1). All data were processed using DENZO and SCALEPACK (Otwinowski and Minor, 1997).

### Structure Determination and Refinement

The structures of SeMet-RelBE-2 and SeMet-RelBE-3 were solved by SAD. The program HKL2MAP (SHELXC, D and E) (Schneider and Sheldrick, 2002; Sheldrick, 2002) was used to determine the substructures and the experimental phases were improved by density modification using the program DM (Cowtan, 1994). Initial models of the RelBE-2 and RelBE-3 complexes were automatically built with ARP/wARP (Perrakis et al., 1999) and phenix.autobuild (Terwilliger et al., 2008), respectively, and additional residues were built manually using the program Coot (Emsley and Cowtan, 2004). The structures were refined with Refmac (Murshudov et al., 1999), for RelBE-2, or phenix.refine (Afonine et al., 2005), for RelBE-3. The structure of the native RelBE-3 complex was solved by molecular replacement with the program Phaser (McCoy et al., 2007) using the SeMet-labeled RelBE-3 structure as a search model. Data collection and refinement statistics are summarized in Table 1. The geometry of the structures was checked using the SAVES Server (http://nihserver.mbi.ucla.edu/SAVES). Structure figures were prepared with PyMOL (The PyMOL Molecular Graphics System version 1.2r3pre, Schrödinger) and structural superpositions with the FATCAT server (Ye and Godzik, 2004).

### Sequence Alignment

Sequence alignments were generated with T-coffee (Notredame et al., 2000) and Expresso (Armougom et al., 2006) with protein sequences obtained from WebTB (http://www.webtb.org).

### Cloning and Expression of *Mtb* Toxin Genes for *M. smegmatis* Toxicity Assays

*M. smegmatis* mc²4517 was used as the expression strain and pYUB1213, derived from pYUB1062 as described in the Supplemental Information, was used as the expression vector (Wang et al., 2010). Plasmids containing individual toxin genes were electroporated into mc²4517 or mc²155. Cells were plated on 7H10 plates containing kanamycin (20 μg/ml), and hygromycin B (100 μg/ml) in the presence and absence of the inducing agent (0.2% [w/v] acetamide). The plates were incubated at 37°C for 3 days and were scored for the presence or absence of colonies in

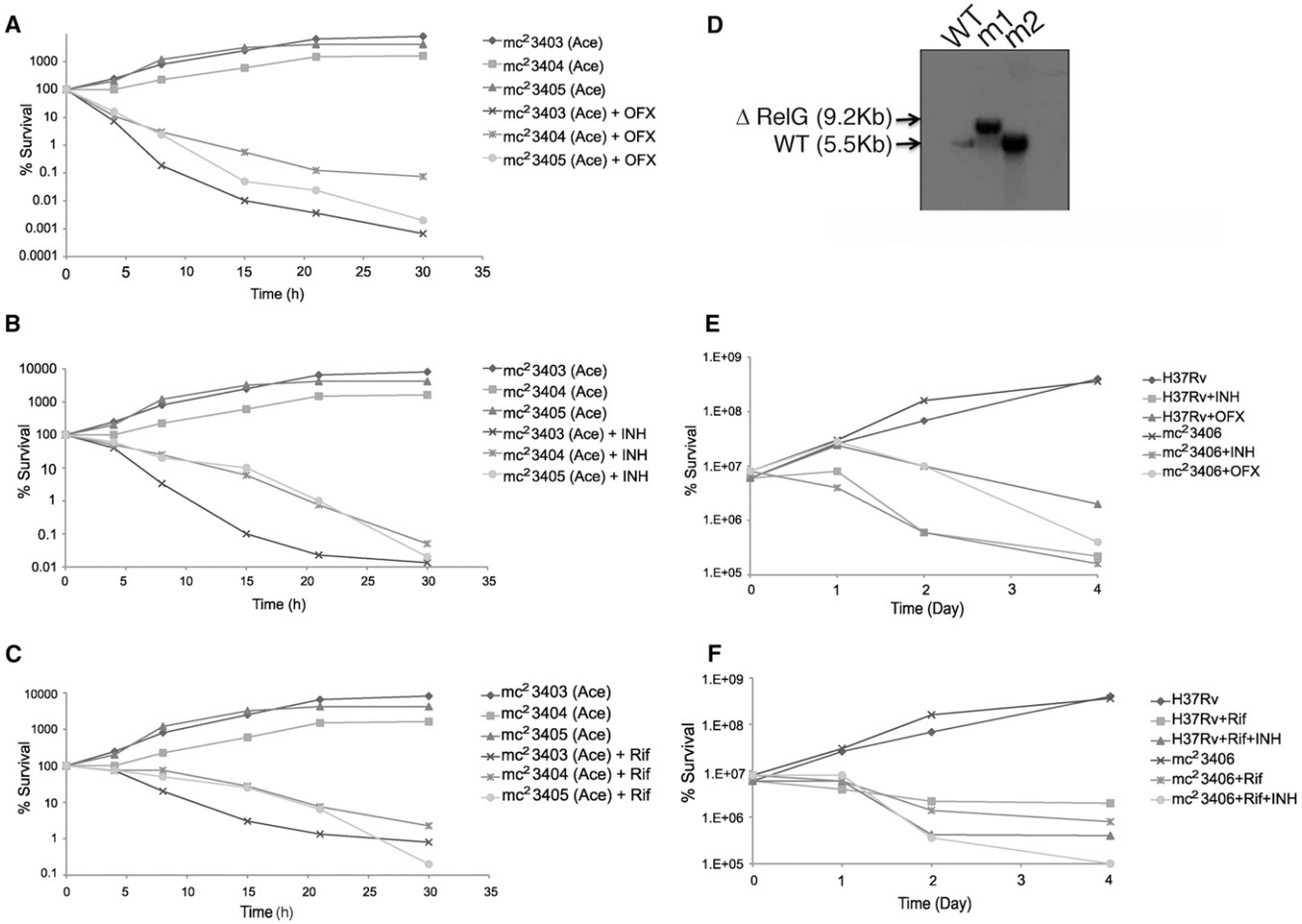


**Figure 6. RelE-2 Confers Drug Tolerance to Mycobacterial Cells**

(A–C) *M. smegmatis* mc²3403, mc²3404, and mc²3405 were treated with (A) OFX, (B) Rif, and (C) INH in the presence and absence of the RelE-2 expression inducer acetamide (Ace).

(D) Southern blot confirming the deletion of *relE-2* in *Mtb* H37Rv (mc²3406). Expected size for H37Rv (WT) and H37Rv Δ*relE-2* are indicated (arrows). *Mtb* H37Rv and Δ*relE-2* strain m1 (mc²3406) were treated with either (E) OFX or INH and with (F) Rif alone or Rif and INH. The death kinetics in the presence of drug is plotted as percent survival with respect to time.

comparison with the pYUB1062 vector control and the colonies obtained from mc²155.

The *relE-2* and *relBE-2* genes were cloned into vector pYUB1485 (containing acetamidase promoter) to generate pYUB1486 and pYUB1487, respectively. The pYUB1485, pYUB1486, and pYUB1487 plasmids were transformed into *M. smegmatis* mc²155 to obtain mc²3403, mc²3404, and mc²3405, respectively. The colonies obtained were grown at 37°C to an $A_{600}$ = 0.5–0.6 in 7H9 medium supplemented with 0.05% Tween 80, 10% OADC, and 0.05% glycerol before induction with 0.2% acetamide. The cells were observed after 12 hr with a microscope at ×100 magnification to compare cell morphology.

### *Mtb* H37Rv Antibiotic Challenge Experiment

To determine killing kinetics overnight cultures of $A_{600}$ = 0.8 were diluted to $A_{600}$ = 0.1 in 10 ml of 7H9 media with and without inducer (acetamide) and treated with INH (100 μg/ml), Rif (100 μg/ml), or OFX (100 μg/ml). The deletion mutant of *relE-2* (mc²3406) was generated in *Mtb* H37Rv using specialized transduction and confirmed by Southern blot (Bardarov et al., 2002). Killing kinetics for *Mtb* H37Rv and *Mtb* mc²3406 were determined by diluting cultures of $A_{600}$ ~0.8 to $A_{600}$ = 0.1 in 10 ml of 7H9 media and treated at the following antibiotic concentrations: INH (1 μg/ml), Rif (5 μg/ml), and OFX (10 μg/ml). All samples were taken at various intervals and various dilutions were plated in triplicate on 7H10 plates to obtain the colony-forming units.

### THP1 and Human Cell Infection Protocol

THP.1 cells were differentiated into adherent macrophages by resuspension in complete RPMI media (Invitrogen, containing 10% fetal bovine serum and 55 mM beta-mercaptoethanol) containing 50 nM PMA (phorbol 12-myristate 13-acetate) at a concentration of 1 million cells per milliliter. After a 24 hr incubation, media was changed to complete RPMI media containing 5% non-heat-inactivated human serum. Adherent THP.1 cells were infected with mycobacteria strains at a multiplicity of infection of 5:1 for 2 hr. Infected THP.1 monolayers were left in complete RPMI media, incubated at 37°C for 72 hr, and then harvested for subG1 analysis.

### SubG1 Analysis of THP.1 Cell Death

An adapted procedure from Riccardi and Nicoletti (2006) was followed. Briefly, at various times postinfection, mycobacteria-infected THP.1 cells were harvested, centrifuged, and fixed in 500 μl ice-cold 70% ethanol and incubated overnight at −20°C. Cells were then resuspended in 200 μl PI staining solution (0.1% Triton X-100, 20 μg/ml propidium iodide, 200 μg/ml RNase A) and analyzed by flow cytometry (BD FACSCalibur) for propidium iodide (FL2) fluorescence.

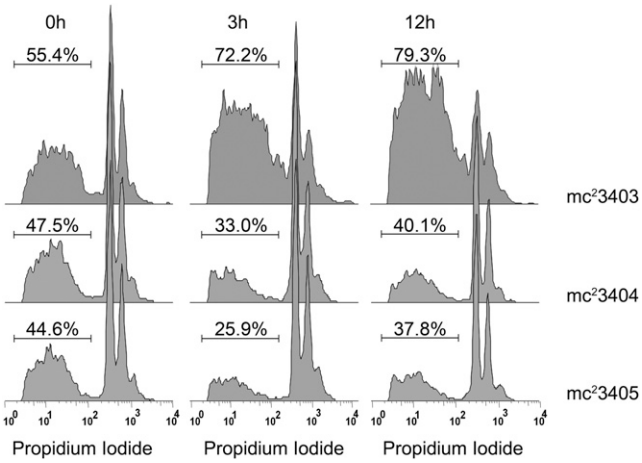


**Figure 7. Overexpression of RelE-2 in *M. smegmatis* Results in Suppression of Cell Death in infected THP.1 Macrophages**

THP.1 cells were infected at a multiplicity of infection of 5:1 with strains mc²3403, mc²3404, and mc²3405 that had been grown for 3 hr or 24 hr in the presence of 0.2% acetamide (to induce RelE-2 expression). At 72 hr post-infection, THP.1 cells were harvested and percent cell death determined by SubG1 analysis and flow cytometry.

## ACCESSION NUMBERS

The atomic coordinates and structure factors for RelBE-2 and RelBE-3 have been deposited in the Protein Data Bank with the accession codes 3G5O and 3OEI, respectively.

## SUPPLEMENTAL INFORMATION

Supplemental Information includes three figures, Supplemental Results, one movie, and three 3D molecular models and can be found with this article online at http://dx.doi.org/10.1016/j.str.2013.02.008.

## ACKNOWLEDGMENTS

This work was supported by National Institutes of Health grants 23616-002-06 F3:02 and TBSGC R01. We thank the staff of the UCLA-DOE X-ray Crystallography Core Facility (supported by Department of Energy grant DE-FC02-02ER63421) for assistance with crystallization screening. The assistance of the staff of NE-CAT beam line 24 ID-C at the Advanced Photon Source is greatly appreciated. This work was supported by HHMI and NIH Grant TBSGC PO1A1O68135.

Received: November 5, 2012
Revised: February 8, 2013
Accepted: February 11, 2013
Published: March 21, 2013

## REFERENCES

Afonine, P.V., Grosse-Kunstleve, R.W., and Adams, P.D. (2005). A robust bulk-solvent correction and anisotropic scaling procedure. Acta Cryst. Dev. Biol. *61*, 850–855.

Anantharaman, V., and Aravind, L. (2003). New connections in the prokaryotic toxin-antitoxin network: relationship with the eukaryotic nonsense-mediated RNA decay system. Genome Biol. *4*, R81.

Arbing, M.A., Handelman, S.K., Kuzin, A.P., Verdon, G., Wang, C., Su, M., Rothenbacher, F.P., Abashidze, M., Liu, M., Hurley, J.M., et al. (2010). Crystal structures of Phd-Doc, HigA, and YeeU establish multiple evolutionary links between microbial growth-regulating toxin-antitoxin systems. Structure *18*, 996–1010.

Armougom, F., Moretti, S., Poirot, O., Audic, S., Dumas, P., Schaeli, B., Keduas, V., and Notredame, C. (2006). Expresso: automatic incorporation of structural information in multiple sequence alignments using 3D-Coffee. Nucleic Acids Res. *34*(Web Server issue), W604–W608.

Bahassi, E.M., Natan, E., Brandt, T., Allen, M.D., Veprintsev, D.B., Robinson, C.V., Chin, J.W., Joerger, A.C., and Fersht, A.R. (2011). Acetylation of lysine 120 of p53 endows DNA-binding specificity at effective physiological salt concentration. Proc. Natl. Acad. Sci. USA *108*, 8251–8256.

Bardarov, S., Bardarov Jr, S., Jr., Pavelka Jr, M.S., Jr., Sambandamurthy, V., Larsen, M., Tufariello, J., Chan, J., Hatfull, G., and Jacobs Jr, W.R., Jr. (2002). Specialized transduction: an efficient method for generating marked and unmarked targeted gene disruptions in *Mycobacterium tuberculosis, M. bovis* BCG and *M. smegmatis*. Microbiology *148*, 3007–3017.

Chauhan, A., Madiraju, M.V.V.S., Fol, M., Lofton, H., Maloney, E., Reynolds, R., and Rajagopalan, M. (2006). *Mycobacterium tuberculosis* cells growing in macrophages are filamentous and deficient in FtsZ rings. J. Bacteriol. *188*, 1856–1865.

Christensen, S.K., and Gerdes, K. (2003). RelE toxins from bacteria and Archaea cleave mRNAs on translating ribosomes, which are rescued by tmRNA. Mol. Microbiol. *48*, 1389–1400.

Christensen, S.K., Mikkelsen, M., Pedersen, K., and Gerdes, K. (2001). RelE, a global inhibitor of translation, is activated during nutritional stress. Proc. Natl. Acad. Sci. USA *98*, 14328–14333.

Christensen, S.K., Maenhaut-Michel, G., Mine, N., Gottesman, S., Gerdes, K., and Van Melderen, L. (2004). Overproduction of the Lon protease triggers inhibition of translation in *Escherichia coli*: involvement of the yefM-yoeB toxin-antitoxin system. Mol. Microbiol. *51*, 1705–1717.

Christensen-Dalsgaard, M., and Gerdes, K. (2008). Translation affects YoeB and MazF messenger RNA interferase activities by different mechanisms. Nucleic Acids Res. *36*, 6472–6481.

Cowtan, K. (1994). "DM": an automated procedure for phase improvement by density modification. Joint CCP4 and ESF-EACBM Newsletter on Protein Crystallography *31*, 34–38.

Dereeper, A., Guignon, V., Blanc, G., Audic, S., Buffet, S., Chevenet, F., Dufayard, J.-F., Guindon, S., Lefort, V., Lescot, M., et al. (2008). Phylogeny.fr: robust phylogenetic analysis for the non-specialist. Nucleic Acids Res. *36*(Web Server issue), W465–W469.

Emsley, P., and Cowtan, K. (2004). Coot: model-building tools for molecular graphics. Acta Crystallogr. D Biol. Crystallogr. *60*, 2126–2132.

Francuski, D., and Saenger, W. (2009). Crystal structure of the antitoxin-toxin protein complex RelB-RelE from *Methanococcus jannaschii*. J. Mol. Biol. *393*, 898–908.

Garcia-Pino, A., Balasubramanian, S., Wyns, L., Gazit, E., De Greve, H., Magnuson, R.D., Charlier, D., van Nuland, N.A.J., and Loris, R. (2010). Allostery and intrinsic disorder mediate transcription regulation by conditional cooperativity. Cell *142*, 101–111.

Gerdes, K., Rasmussen, P.B., and Molin, S. (1986). Unique type of plasmid maintenance function: postsegregational killing of plasmid-free cells. Proc. Natl. Acad. Sci. USA *83*, 3116–3120.

Hinchey, J., Lee, S., Jeon, B.Y., Basaraba, R.J., Venkataswamy, M.M., Chen, B., Chan, J., Braunstein, M., Orme, I.M., Derrick, S.C., et al. (2007). Enhanced priming of adaptive immunity by a proapoptotic mutant of *Mycobacterium tuberculosis*. J. Clin. Invest. *117*, 2279–2288.

Holm, L., and Sander, C. (1995). Dali: a network tool for protein structure comparison. Trends Biochem. Sci. *20*, 478–480.

Kamada, K., and Hanaoka, F. (2005). Conformational change in the catalytic site of the ribonuclease YoeB toxin by YefM antitoxin. Mol. Cell *19*, 497–509.

Kedzierska, B., Lian, L.Y., and Hayes, F. (2007). Toxin-antitoxin regulation: bimodal interaction of YefM-YoeB with paired DNA palindromes exerts transcriptional autorepression. Nucleic Acids Res. *35*, 325–339.

 

Keren, I., Shah, D., Spoering, A., Kaldalu, N., and Lewis, K. (2004). Specialized persister cells and the mechanism of multidrug tolerance in *Escherichia coli*. J. Bacteriol. *186*, 8172–8180.

Korch, S.B., Contreras, H., and Clark-Curtiss, J.E. (2009). Three *Mycobacterium tuberculosis* Rel toxin-antitoxin modules inhibit mycobacterial growth and are expressed in infected human macrophages. J. Bacteriol. *191*, 1618–1630.

Kumar, P., Issac, B., Dodson, E.J., Turkenburg, J.P., and Mande, S.C. (2008). Crystal structure of *Mycobacterium tuberculosis* YefM antitoxin reveals that it is not an intrinsically unstructured protein. J. Mol. Biol. *383*, 482–493.

Li, G.Y., Zhang, Y., Inouye, M., and Ikura, M. (2008). Structural mechanism of transcriptional autorepression of the *Escherichia coli* RelB/RelE antitoxin/toxin module. J. Mol. Biol. *380*, 107–119.

Maisonneuve, E., Shakespeare, L.J., Jørgensen, M.G., and Gerdes, K. (2011). Bacterial persistence by RNA endonucleases. Proc. Natl. Acad. Sci. USA *108*, 13206–13211.

Makarova, K.S., Wolf, Y.I., and Koonin, E.V. (2009). Comprehensive comparative-genomic analysis of type 2 toxin-antitoxin systems and related mobile stress response systems in prokaryotes. Biol. Direct *4*, 19.

McCoy, A.J., Grosse-Kunstleve, R.W., Adams, P.D., Winn, M.D., Storoni, L.C., and Read, R.J. (2007). Phaser crystallographic software. J. Appl. Cryst. *40*, 658–674.

Miallau, L., Faller, M., Chiang, J., Arbing, M., Guo, F., Cascio, D., and Eisenberg, D. (2009). Structure and proposed activity of a member of the VapBC family of toxin-antitoxin systems. VapBC-5 from Mycobacterium tuberculosis. J. Biol. Chem. *284*, 276–283.

Min, A.B., Miallau, L., Sawaya, M.R., Habel, J., Cascio, D., and Eisenberg, D. (2012). The crystal structure of the Rv0301-Rv0300 VapBC-3 toxin-antitoxin complex from *M. tuberculosis* reveals a Mg(2+) ion in the active site and a putative RNA-binding site. Protein Sci. *21*, 1754–1767.

Murshudov, G.N., Vagin, A.A., Lebedev, A., Wilson, K.S., and Dodson, E.J. (1999). Efficient anisotropic refinement of macromolecular structures using FFT. Acta Crystallogr. D Biol. Crystallogr. *55*, 247–255.

Neubauer, C., Gao, Y.-G., Andersen, K.R., Dunham, C.M., Kelley, A.C., Hentschel, J., Gerdes, K., Ramakrishnan, V., and Brodersen, D.E. (2009). The structural basis for mRNA recognition and cleavage by the ribosome-dependent endonuclease RelE. Cell *139*, 1084–1095.

Notredame, C., Higgins, D.G., and Heringa, J. (2000). T-Coffee: a novel method for fast and accurate multiple sequence alignment. J. Mol. Biol. *302*, 205–217.

Ogura, T., and Hiraga, S. (1983). Mini-F plasmid genes that couple host cell division to plasmid proliferation. Proc. Natl. Acad. Sci. USA *80*, 4784–4788.

Otwinowski, Z., and Minor, W. (1997). Processing of X-ray diffraction data collected in oscillation mode. Methods Enzymol. *276*, 307–326.

Pandey, D.P., and Gerdes, K. (2005). Toxin-antitoxin loci are highly abundant in free-living but lost from host-associated prokaryotes. Nucleic Acids Res. *33*, 966–976.

Pedersen, K., Zavialov, A.V., Pavlov, M.Y., Elf, J., Gerdes, K., and Ehrenberg, M. (2003). The bacterial toxin RelE displays codon-specific cleavage of mRNAs in the ribosomal A site. Cell *112*, 131–140.

Perrakis, A., Morris, R., and Lamzin, V.S. (1999). Automated protein model building combined with iterative structure refinement. Nat. Struct. Biol. *6*, 458–463.

Ramage, H.R., Connolly, L.E., and Cox, J.S. (2009). Comprehensive functional analysis of *Mycobacterium tuberculosis* toxin-antitoxin systems: implications for pathogenesis, stress responses, and evolution. PLoS Genet. *5*, e1000767.

Riccardi, C., and Nicoletti, I. (2006). Analysis of apoptosis by propidium iodide staining and flow cytometry. Nat. Protoc. *1*, 1458–1461.

Schneider, T.R., and Sheldrick, G.M. (2002). Substructure solution with SHELXD. Acta Crystallogr. D Biol. Crystallogr. *58*, 1772–1779. . Published online Sep 28, 2002.

Shaw, N., Cheng, C., and Liu, Z.-J. (2007). Procedure for reductive methylation of protein to improve crystallizability (Protocol Exchange).

Sheldrick, G.M. (2002). SHELXE. Z. Kristallogr. *217*, 644–650.

Takagi, H., Kakuta, Y., Okada, T., Yao, M., Tanaka, I., and Kimura, M. (2005). Crystal structure of archaeal toxin-antitoxin RelE-RelB complex with implications for toxin activity and antitoxin effects. Nat. Struct. Mol. Biol. *12*, 327–331.

Terwilliger, T.C., Grosse-Kunstleve, R.W., Afonine, P.V., Moriarty, N.W., Zwart, P.H., Hung, L.-W., Read, R.J., and Adams, P.D. (2008). Iterative model building, structure refinement and density modification with the PHENIX AutoBuild wizard. Acta Crystallogr. D Biol. Crystallogr. *64*, 61–69.

Thompson, J.D., Higgins, D.G., and Gibson, T.J. (1994). CLUSTAL W: improving the sensitivity of progressive multiple sequence alignment through sequence weighting, position-specific gap penalties and weight matrix choice. Nucleic Acids Res. *22*, 4673–4680.

Van Duyne, G.D., Standaert, R.F., Karplus, P.A., Schreiber, S.L., and Clardy, J. (1993). Atomic structures of the human immunophilin FKBP-12 complexes with FK506 and rapamycin. J. Mol. Biol. *229*, 105–124.

Van Melderen, L., Bernard, P., and Couturier, M. (1994). Lon-dependent proteolysis of CcdA is the key control for activation of CcdB in plasmid-free segregant bacteria. Mol. Microbiol. *11*, 1151–1157.

Vázquez-Laslop, N., Lee, H., and Neyfakh, A.A. (2006). Increased persistence in *Escherichia coli* caused by controlled expression of toxins or other unrelated proteins. J. Bacteriol. *188*, 3494–3497.

Wang, F., Jain, P., Gulten, G., Liu, Z., Feng, Y., Ganesula, K., Motiwala, A.S., Ioerger, T.R., Alland, D., Vilchèze, C., et al. (2010). *Mycobacterium tuberculosis* dihydrofolate reductase is not a target relevant to the antitubercular activity of isoniazid. Antimicrob. Agents Chemother. *54*, 3776–3782.

Ye, Y., and Godzik, A. (2004). FATCAT: a web server for flexible structure comparison and structure similarity searching. Nucleic Acids Res. *32*(Web Server issue), W582–W585.

Zhang, Y., and Inouye, M. (2009). The inhibitory mechanism of protein synthesis by YoeB, an *Escherichia coli* toxin. J. Biol. Chem. *284*, 6627–6638.

Zhang, Y., Zhang, J., Hoeflich, K.P., Ikura, M., Qing, G., and Inouye, M. (2003). MazF cleaves cellular mRNAs specifically at ACA to block protein synthesis in *Escherichia coli*. Mol. Cell *12*, 913–923.